BNL-106323-2014-CP

Ceramic-Ferrite damper for the BNL superconducting RF electron gun cavity

H. Hahn[1], I. Ben-Zvi[1,2], S. Belomestnyk[1,2], L. Hammons[1], V. Litvinenko[1,2], Y. R. Than[1], R. Todd[1], D. Weiss[1], W. Xu[1],

[1]Brookhaven National Laboratory, Upton, NY 11973 USA
[2]Physics and Astronomy Department, Stony Brook University, Stony Brook, NY 11794 USA

Presented at the The 55th ICFA Advanced Beam Dynamics Workshop on High Luminosity Circular e+e- Colliders – Higgs Factory (HF2014)
Hotel Wanda Realm, Beijing, China
October 9 – 12, 2014

October 2014

Collider-Accelerator Department

Brookhaven National Laboratory

U.S. Department of Energy
Office of Science, Office of Nuclear Physics

Notice: This manuscript has been authored by employees of Brookhaven Science Associates, LLC under Contract No. DE-AC02-98CH10886 with the U.S. Department of Energy. The publisher by accepting the manuscript for publication acknowledges that the United States Government retains a non-exclusive, paid-up, irrevocable, world-wide license to publish or reproduce the published form of this manuscript, or allow others to do so, for United States Government purposes.

This preprint is intended for publication in a journal or proceedings. Since changes may be made before publication, it may not be cited or reproduced without the author's permission.

DISCLAIMER

This report was prepared as an account of work sponsored by an agency of the United States Government. Neither the United States Government nor any agency thereof, nor any of their employees, nor any of their contractors, subcontractors, or their employees, makes any warranty, express or implied, or assumes any legal liability or responsibility for the accuracy, completeness, or any third party's use or the results of such use of any information, apparatus, product, or process disclosed, or represents that its use would not infringe privately owned rights. Reference herein to any specific commercial product, process, or service by trade name, trademark, manufacturer, or otherwise, does not necessarily constitute or imply its endorsement, recommendation, or favoring by the United States Government or any agency thereof or its contractors or subcontractors. The views and opinions of authors expressed herein do not necessarily state or reflect those of the United States Government or any agency thereof.

Ceramic-Ferrite damper for the BNL Superconducting RF electron gun cavity

H. Hahn[1], I. Ben-Zvi[1,2], S. Belomestnyk[1,2], L. Hammons[1], V. Litvinenko[1,2],

Y. R. Than[1], R. Todd[1], D. Weiss[1], Wencan Xu[1],

[1] Brookhaven National Laboratory, Upton, NY 11973, USA,

[2] Physics and Astronomy Department, Stony Brook University, Stony Brook, 11794, USA

The Brookhaven Energy Recovery Linac is operated as R&D test bed for high-current, high-charge electron beams. It comprises a superconducting five-cell cavity and a half-cell Superconducting RF photo-injector electron gun. Achieving the performance objectives requires effective higher order mode damping in the linac and gun cavities. Among the various alternative solutions, beam-tube type dampers were adopted for the five-cell accelerator cavity and the half-cell gun cavity. The damper for the electron gun consists of a lossless ceramic break surrounded by damping ferrite tiles. This design is innovative in its damper approach and combines a variety of goals including broadband HOM damping and protection of the superconducting cavity vacuum from potential damage by the separately cooled absorber. The damper properties are described by the coupling impedance presented to a traversing beam and the *Q* reduction of selected gun cavity resonances. The gun impedance properties are numerically analyzed in terms of radial waveguide modes. The cavity HOM damping is presented by the measured *Q*-values of the cavity at superconducting temperatures obtained first for the bare cavity and then with the ceramic ferrite damper added.

PACS:

1. INTRODUCTION

An ampere-class 20 MeV superconducting Energy Recovery Linac (ERL) was created to test various concepts relevant to the envisioned future projects for this laboratory [1,2]. The primary goal for the ERL is high current, high charge electron beams albeit with low emittance from the high voltage superconducting cavities, making HOM mode damping an implicit necessity. The ERL consists of a superconducting (SC) five-cell ~704 MHz accelerator cavity plus a photo injector in the form of a SC half-cell RF cavity [3]. The ERL accelerating cavity can be operated in a pulsed “quasi-CW” mode up to 20 MV/m, and at 12 MV/m in CW mode. [4] The gun is designed to operate in two alternate modes, delivering high current of 300 mA with ~0.7 nC per bunches at a rate of 704 MHz or delivering high charge per bunch of 5 nC at a 10 MHz rate in the 50 mA current [5]. The facility is presently

undergoing commissioning and once accomplished, its ERL components will find use for further accelerator improvement projects.

In addition to voltage and current goals, the ERL provides for the investigation of transverse and longitudinal instabilities caused by HOMs in the superconducting cavities. The HOM damping in the accelerator cavity had first been demonstrated in the copper cavity model at room temperature and then was also confirmed in the SC ERL cavity [6,7]. The HOMs in the accelerator cavity are absorbed with a beam line ferrite damper at room temperature. Its design followed the techniques developed at Cornell [8] and KEKB [9] for ferrite absorbers and the absorbers were fabricated by industry according to Cornell-print [10].

The search for alternate dampers, influenced by the concern about Q reduction from particulates and in part by the availability of surplus ferrite tiles, lead to the concept of a ceramic break (CB) surrounded by an ferrite absorber [11] as shown in Fig. 1. The insertion of an alumina oxide break provides separation of the ferrite tiles from the gun vacuum ensuring its high vacuum and the absence of particulates reaching the niobium surface. Initial studies of this configuration justified its adoption for the SC ERL gun [12]. The placement of the Ceramic-Ferrite Damper in the electron gun is shown in Fig 2 and details of the CFD design and its preparation for installation are presented in the next section.

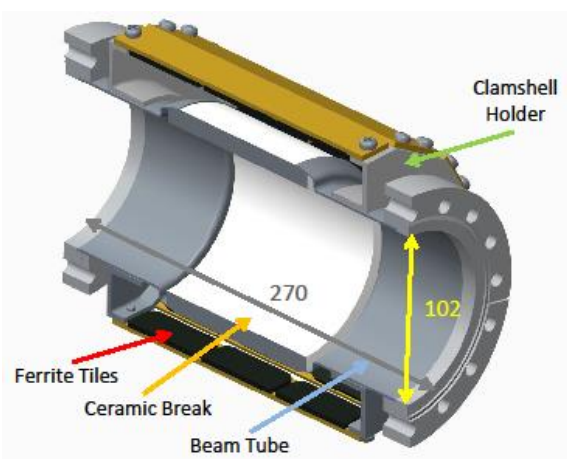

Figure 1. Ceramic Break covered with ferrite absorber (in cm)

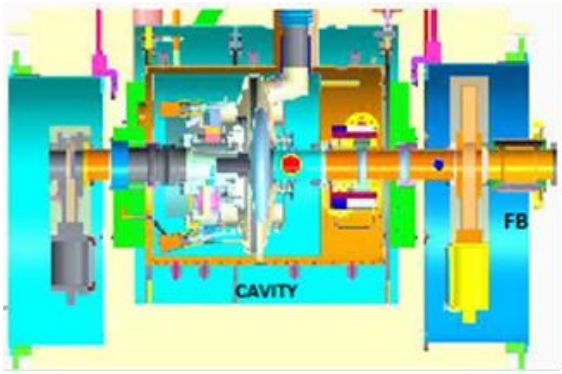

Figure. 2. SC RF gun cavity assembled in the gun cryostat

The primary function of the CFD is damping of the gun cavity HOMs. The damper properties are best described by the external quality factor that constrain the unloaded mode Q_0's. However, the Q-external depends strongly on the damper distance from the cavity, the cut off frequencies of the beam tube and the state of the vacuum valve, so that transportable values could not have been generated. For a comparison with other multi-layer beam line dampers portable damper properties are provided in terms of the wave or surface impedance at the gap in the beam tube. The CFD impedance is derived in the Section 3 from a field analysis based on radial transmission matrices [13]. The actual measurements of the HOM resonances at SC temperatures with the CB covered by the ferrite tiles are described in Section 4. The potential impact on the gun beam is found via computer simulation of R/Q values and the paper concludes with a short summary of the of CB merits.

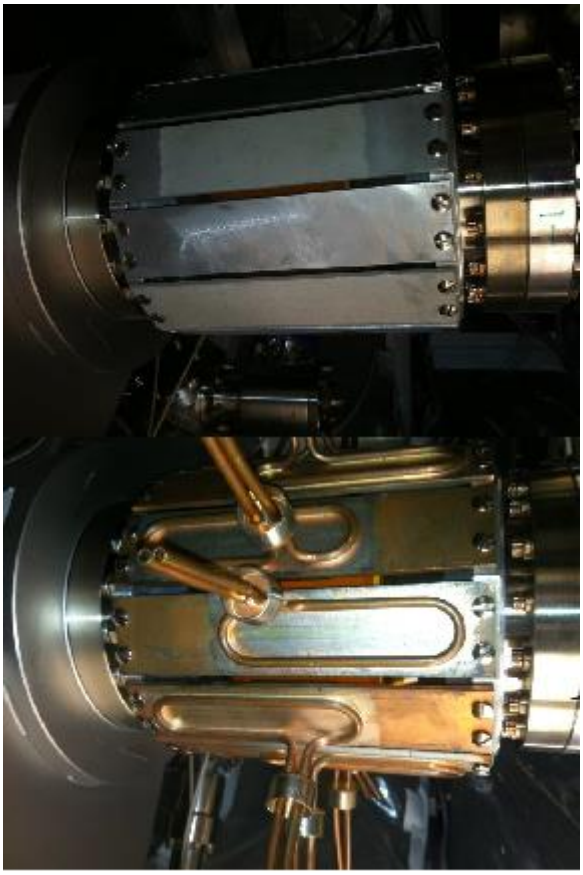

Figure 3: Ceramic break with stainless and ferrite absorber plates.

2. THE CERAMIC FERRITE DAMPER

The Assembled SC RF gun cavity is shown in Fig 2 where the relevant components, RF cavity, vacuum valve, and ceramic break are identified. The CB damper concept allows the application of different covers over the beam tube break, with stainless steel plates or ferrite absorber plates shown as examples in Fig. 3. The ceramic cylinder in the break, intended to be lossless, is achieved with an aluminum oxide tube (92% Alumina) terminated with stainless steel cuffs so that essentially all damping is due to the ferrite.

Ultra-high and dust-free vacuum is essential in the vicinity of the superconducting cavities to maintain highly stable CW gun operation. Preventing electron charge accumulation on the ceramic mandates a ceramic coating with Non-Evaporable Getter (NEG) films. Producing a film as thin as possible to allow HOM waves to traverse the ceramic represents a challenge. Transmission of power between the wave impedance defined as $Z_g = E_z / H_\varphi$ seen at the gap to the wall impedance Z_b of the absorber is found

by radial transmission analysis and leads to the condition of $Z_0\sigma\Delta \ll 1$ where Z_0, σ, Δ are the free space impedance, coating conductivity and thickness respectively. Given that the coating thickness needs to be unmeasurably thin, the condition is translated into a measurable resistance across the break, $R_b \gg \ell/(2\pi b\sigma\Delta)$ where ℓ and b are the length and radius of the ceramic tube.

A further requirement on the CB is electrical continuity between coating and beam tube. The coating film is in the present unit connected to the metal cuffs by spring finger rings which could be avoided by pre-coating the ceramic with MoMn+Ni bands as shown in Fig. 4.

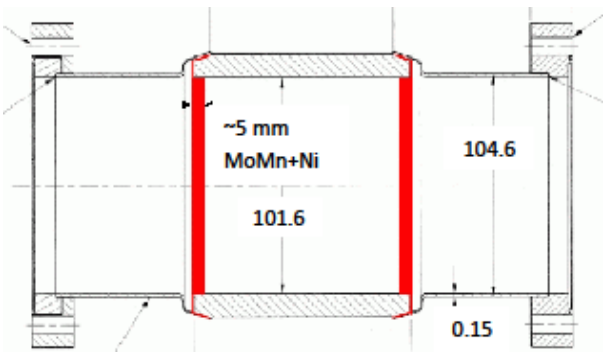

Figure 4. Ceramic break to be coated.

The ceramic cylinder was coated with Type 321 stainless using magnetron sputtering as coating method. The goal for the coating was set at a thickness from 45 to 90 Å together with a DC impedance above ~ 100 kΩ. Maintaining electrical resistivity of the coating, when exposed to atmospheric oxygen, is one of the more challenging tasks. The end-to-end resistance of the ceramic coating was initially 150 kΩ and after venting to atmosphere reached ~10 MΩ. After approximately two months under storage vacuum, a hypot test at 1 kVDC measured the film resistance as an acceptable ~600 MΩ. The ceramic break was then kept under storage vacuum and the time at atmosphere was minimized during installation.

The ferrite HOM absorber was obtained from industry using the nickel-zinc ferrite C-48 tiles. Three ferrite tiles each of 50.8 × 38.1 ×3.18 mm dimensions are soldered to tungsten-copper composite 10W3 Elkonite plates. The CB unit has room for 12 plates forming a cylindrical 16 cm i.d. ferrite spool over the 10 cm diameter ceramic tube. The plates are placed on the ceramic tube cuff links with metallic clamshell holders. RF leakage between the ferrite plates is prevented by narrow metal stripes.

In normal operation of the ERL cavity, the absorber is at room temperature but can be water cooled through tubes soldered to the plates. Changing the radial size of the holder remains an option to simplify cooling requirements. The spatial separation of the CB damper from the gun in the cryomodule allows baking of the niobium cavity to improve *Q*-slope performance if necessary, and alternatively also baking of the damper together with the beam tube to reach high beam tube vacuum.

3, WAVE IMPEDANCE OF A CERAMIC BREAK.

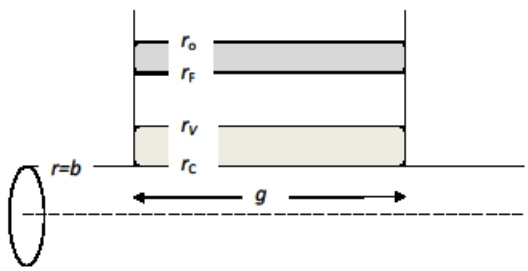

Figure 5: Radial transmission model of the CFD

The multi-layer "Ceramic-Ferrite Damper", shown in Fig. 1, can be simplified for analysis into an axially limited structure breaking an unlimited beam tube as shown in Fig. 5. The electromagnetic properties of straight multi-layer beam tubes have been treated by many authors with the axial transmission line solution [14]. The short axial length and the presence of the metallic boundary disks points to the treatment as a structure with a radial sequence of circular symmetric layers. The layer properties are defined for the analysis via the Wolfram Mathematica program as matrices in a "radial" transmission line in analogy to the axial matrix solution [15]. The immediate goal for the analysis is producing the wall or surface impedance of the damper at the beam tube radius, *b*. The break allows radial propagation of orthogonal radial waves functions resulting in separate impedance values, $Z_b = E_z / H_\varphi$ and E_φ / H_z for TM and TE waves respectively [16].

The longitudinal or transverse coupling impedance seen by an axial beam is determined solely by the TM field with respect to in the damper axis. In contrast, in its function as HOM damper, the field in the damper is coupled to the gun resonances via the stationary beam tube modes and the external Q is caused by the power loss on the wall impedance of the disks. The gun resonance damping is provided both by TM and TE modes but at frequencies below the TM_{01} cutoff, the dipole damping is preferentially due to the TE_{11} mode. Finding the damper modes is conveniently done for the TE and TM fields propagating radially within each layer and concatenation of their matrices as detailed in the Appendix. As a consequence of the E (TM) and H (TE) mode orthogonality, separate matrices are used for these modes. The "E" matrix for a layer, ranging from one radius, r within the layer inclusive of the inner boundary, r_i, to the reference radius at the outer layer boundary, r_0, is defined in the general form

$$\begin{pmatrix} E_z(r) \\ H_\varphi(r) \end{pmatrix} = M^E(r, r_0) \begin{pmatrix} E_z(r_0) \\ H_\varphi(r_0) \end{pmatrix}$$
$$= \begin{bmatrix} m^E_{ee}(r, r_0) & m^E_{eh}(r, r_0) \\ m^E_{he}(r, r_0) & m^E_{hh}(r, r_0) \end{bmatrix} \begin{pmatrix} E_z(r_0) \\ H_\varphi(r_0) \end{pmatrix}$$

The "H" matrix follows correspondingly as

$$\begin{pmatrix} E_\varphi(r) \\ H_z(r) \end{pmatrix} = M^H(r,r_0)\begin{pmatrix} E_\varphi(r_0) \\ H_z(r_0) \end{pmatrix}$$
$$= \begin{bmatrix} m_{ee}^H(r,r_0) & m_{eh}^H(r,r_0) \\ m_{he}^H(r,r_0) & m_{hh}^H(r,r_0) \end{bmatrix}\begin{pmatrix} E_z(r_0) \\ H_\varphi(r_0) \end{pmatrix}$$

The orthogonal field components at the inner radius of a layer must be summed over the individual modes identified with *n* for their axial dependence.

$$\begin{pmatrix} E(r_i) \\ H(r_i) \end{pmatrix} = \begin{pmatrix} \sum_n E_n(r_i) \\ \sum_n H_n(r_i) \end{pmatrix} = \sum_n M_n(r_i,r_o)\begin{pmatrix} E_n(r_o) \\ H_n(r_o) \end{pmatrix}$$

In the case of several layers, the modes propagate uncoupled through the layers and the overall matrix is obtained by matrix multiplication of the individual matrices. The surface/radial wave impedances of a multi-layer but finite structure is written at $b = r_c$ for both TE and TM waves as

$$Z_b = \frac{M_{ee}(r_c,r_o)Z(r_o) - M_{eh}(r_c,r_o)}{M_{hh}(r_c,r_o) - M_{he}(r_c,r_o)Z(r_o)}$$

which is reduced by a perfectly conducting outer tube to

$$Z(r_c) = -M_{eh}(r_c,r_o)/M_{hh}(r_c,r_o)$$

In a material with uniform ε and μ, the radially propagating fields are derived in terms of Hankel functions from the potential [17]

$$\begin{Bmatrix} u^{TM} \\ u^{TE} \end{Bmatrix} = \begin{Bmatrix} \cos k_{zn} \\ \sin k_{zn} \end{Bmatrix} \cos(m\varphi) \begin{Bmatrix} H_m^{(1)}(\nu_n r) \\ H_m^{(2)}(\nu_n r) \end{Bmatrix}, \quad \begin{Bmatrix} n = 0,1,2... \\ n = 1,2,3... \end{Bmatrix},$$

where $k = \omega / c$, $k_{zn} = n\pi / g$ and $\nu_n = \sqrt{\varepsilon\mu k^2 - k_{zn}^2}$.

The damper material parameters are $\varepsilon = 9$ for the 12 mm thick Alumina tube and $\varepsilon = 13$ for the 4 mm ferrite bricks with their permeability measured in the ERL cavity damper as $\mu = 29/(1 + j2.5 f_{GHz})$ [6]. In Fig, 6, this analytical μ approximation is compared with the measurements by Mouris and Hutcheon (MH) that were obtained from small C-48 ferrite samples [18]. As shown in Fig. 6, sufficient agreement is found from 915 to 2800 MHz the range that is relevant to the gun damper. In this range the μ values from the MH data points can be fitted for use in numerical impedance estimates by the Wolfram Mathematica 7.0 program [18] as

$$\mu \approx (17.82 - 21.38 f + 9.31 f^2 - 1.37 f^3) - j(31.7 - 30.19 f + 11.71 f^2 - 1.683 f^3)$$

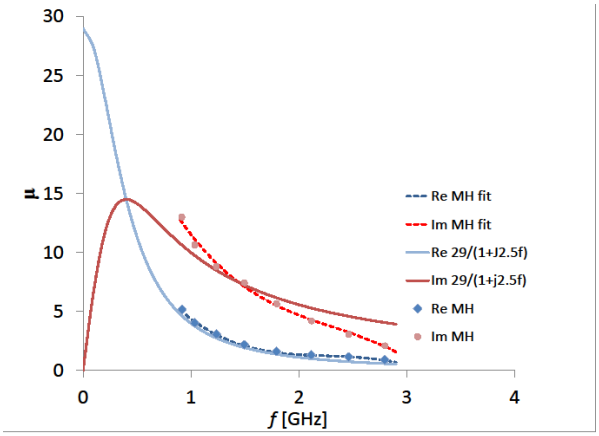

Figure 6: Permeability of C48 ferrite

As numerical demonstration, the longitudinal coupling impedance of a 4 mm thick ferrite layer with inner radius $b = 5$ cm and perfect outer shield is calculated with Mathematica using the analytic and the fitted MH data. The Fig. 7 shows good agreement of the curves for the real part and is qualitatively sufficient for the imaginary part of the impedance over the damper range. In fact, the results indicate the damping possibility of a ferrite layer used in the ERL cavity damper without the ceramic break and serve as reference. The TM real (red) and imaginary (blue) surface impedance at the CFD is shown in Fig. 8 for the ferrite located at the outer radius above the ceramic (solid) and) and at the beam tube radius without ceramic (dashed). Not surprisingly, he imaginary impedance (solid blue in Fig. 8) is strongly altered It is noted also that the vacuum benefits of the ceramic reduce the damping to some degree (red doilid).

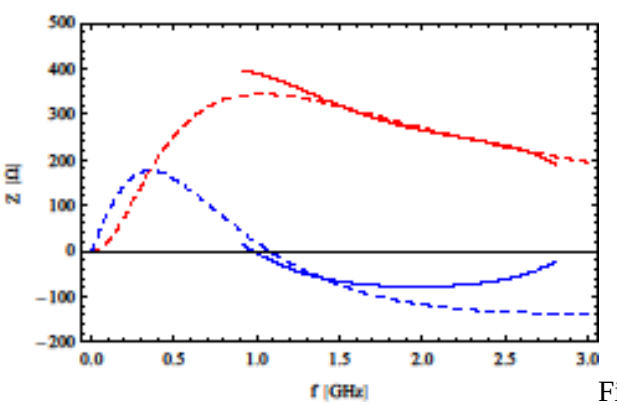

Figure 7: Real and imaginary impedance of a 4 mm thick ferrite layer at beam tube radius with a plausible approximation for the permeability (dashed) and measured MH data points (solid curve).

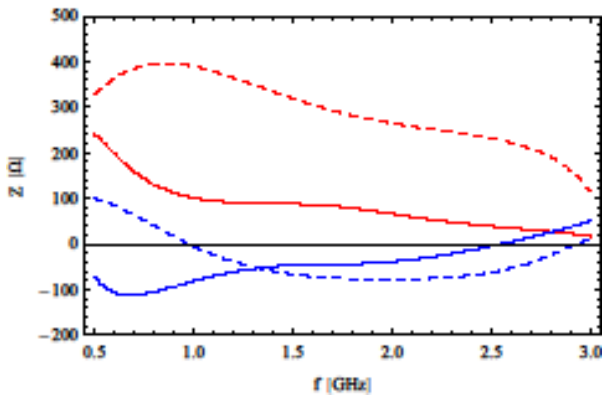

Figure 8: The TM real (red) and imaginary (blue) surface impedance at the CF damper break for the ferrite in the outer radius above the ceramic (solid) and at the beam tube radius without ceramic (dashed). The vacuum benefits of the ceramic reduce the damping to some degree.

The ERL gun cavity damping function of the CF damper depends primarily on the coupling via their connecting beam tube. The cutoff frequency of the 10 cm diameter tube is ~1.758 GHz for the TE11 dipole and ~2.297 GHz for the TM01 monopole. The center- center spacing of the damper from the cavity is ~ 90 cm center and is interrupted by the fundamental power coupler and a vacuum gate. With the gate opened , the lowest intrinsic cavity monopole mode to reach the damper is at 2.239 GHz and the lowest dipole mode at 2.256 GHz.

The damping of the resonances can be estimated by the radial wave impedance at the CF damper gap, $r = b$ as calculated with Mathematica. In Fig. 9, the real and imaginary impedance is shown as solid and dashed lines respectively for the first term of the TE ($n = 1$) and TM ($n = 0$) impedances. A numerical similarity is noted which avoids the need for a lengthy TE expansion similar to Fig. 8.

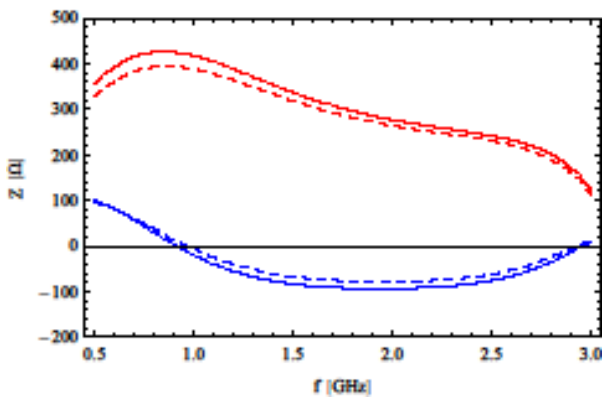

Figure 9: The real (red) and imaginary (blue) surface impedance at the TE (solid) and TM (dashed) modes of a ferrite layer at the beam tube radius.

3. HOM measurements and data

The primary function of the CFB is damping of the gun HOMs of the ERL electron gun. All Q measurements were done with a network analyser based on the standard 3 dB S_{21} transmission method. This paper is based on a so far limited number of Q measurements at SC temperatures that have been performed on the bare gun cavity in vertical tests and then after its installation at the ERL. Additional results were obtained from a second half cell cavity of identical geometry but fabricated from large-grain

niobium. The first data for the ERL cavity was gained in the vertical test facility (VTF) test at JLAB with the results shown in Fig. 10 together with the corresponding values for the Large Grain Cavity in the BNL VTF. The VTF measurements were performed with a stationary pickup probe and an adjustable power coupler shown in Fig. 11.

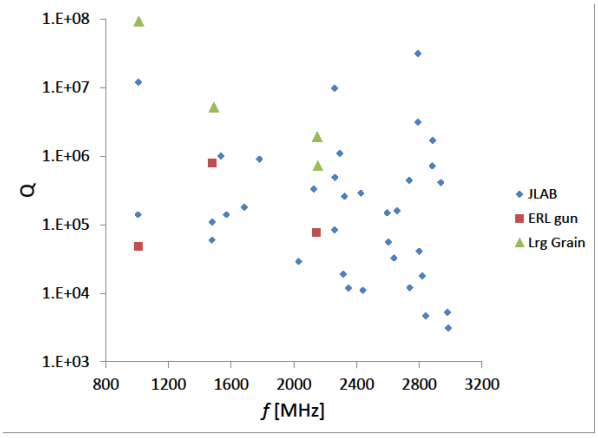

Figure 10: Quality factor results for the superconducting electron gun cavity at ~ 2 K.

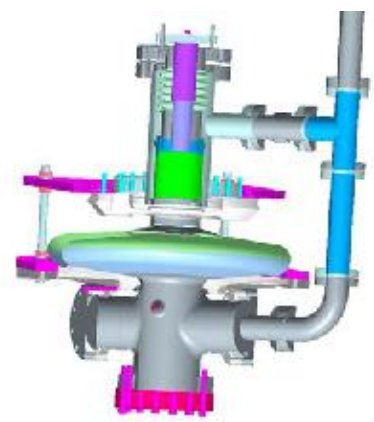

Figure 11: Gun cavity assembly for the VTF test.

When installed in the ERL gun Dewar, the *Q* measurements of the "small grain" ERL cavity are done between pickup (PU) probe and the fundamental power coupler (FPC) , the latter seen in Fig. 12. The FPC is a dual-feed coupling system composed of two coaxial type power couplers, two three-stub waveguide phase shifters, located symmetrically in each arm of the coupling system, and a waveguide shunt-T RF power splitter. The two couplers are located opposite to each other on the cavity beam pipe to minimize the transverse beam kick and associated emittance growth. The dipole cavity resonances are typically split and the S_{21} curves can have non-standard shapes but can easily be analysed [20]. The dual-feed coupler allows shifting one arm to change the resonance frequency by up to ~1 MHz resulting in a multitude of curves and apparently different *Q*-values as seen in Fig. 13. The accuracy of the results for the highest *Q*s requires good control of the cooling helium temperature and pressure. The dipole resonance at ~1.008 GHz is indicated in Fig 10 with a Q of 51,000 as one of the reference points.

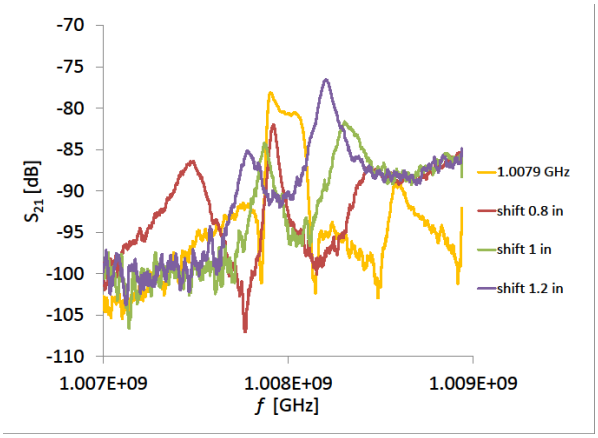

Figure 12: Network analyser S_{21} transmission data with phase changes in the FPC.

The potential damping capability of the FPC in the ERL gun cavity was checked for this paper along with the study of HOM damping by the ferrite break. Previous simulation and experimental measurements of the large grain cavity at room temperature had indicated that the cavity, through the 12 cm opening, radiates into the FPC so that many HOMs are damped [21]. Measurements through S_{21} transmission from the waveguide port to pickup were taken only up to 2.2 GHz. The measurement results for the first three HOMs are shown in Fig. 10 next to the VTF *Q*s of the unencumbered large grain cavity. The three ERL Q values at ~2 K evidence FPC damping. In contrast, the monopole at 1.47 GHz retained its undamped Q of ~800,000, possibly because the damping capability of the FPC is here impacted by its doorknob configuration and causing a limited signal transmission.

The electron beam is laser generated in the cavity where its properties of energy spread and transverse emittance are determined by the main field at the cathode but are affected by the HOMs, mainly the lower dipole and monopole modes. Achieving the design goals depends on sufficient HOM suppression. A limited number of modes in the cavity with the FPC have been measured to confirm damping by the ceramic-ferrite break. One example demonstrating the q change from 70,000 to 11,000 is shown in Fig, 14.

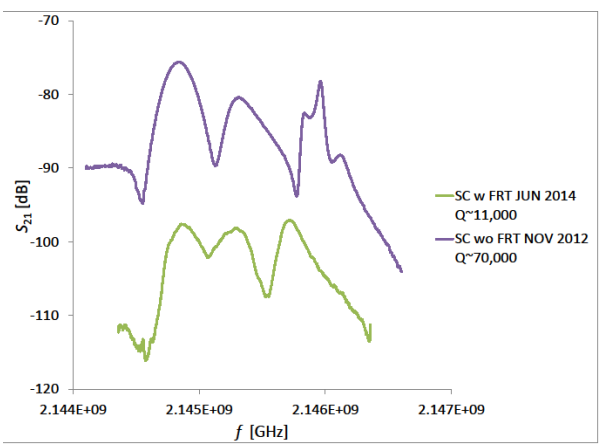

Figure 13: Dipole resonance at 2.145 GHz damped by the ceramic-ferrite break from Q~72,000 to 11,000.

Identifying the exact source of damping, either by the MFC or the ferrite damper, requires three measurements of Q changes against the bare cavity, first with the vacuum gate closed, second with the ceramic break without ferrite, and third with the ferrite added. In order to assure consistency and in spite of the cavity concatenation to the MFC, the relevant modes are best identified within ± 1 MHz against their frequency in the bare cavity identified as LG in reference Fig. 10. The Q-values in Table 1 clearly locate the damping sources and especially confirm the ferrite damping searched in this paper.

(NOTE to the editor > the measurement are presently performed and will be forwarded)

Table 1. Changes of Q values in the ERL gun cavity by FPC and CFB

mode	f [GHz]	Q -bare	Q-MFC	Q-open	Q-w frt
TM11	1.0105	9.2E7			
TM02	1.4888	5.1E6			
	2.1484	1.9E6			
	2.1521	7.2E5			